PCCP

RSC Publishing

PAPER

View Article Online
View Journal | View Issue

Cite this: *Phys. Chem. Chem. Phys.*, 2013, **15**, 14319

Limitations and high pressure behavior of MOF-5 for CO_2 capture

Joo Young Jung,†[a] Ferdi Karadas,†[b] Sonia Zulfiqar,†[ac] Erhan Deniz,[b] Santiago Aparicio,[d] Mert Atilhan,*[b] Cafer T. Yavuz*[a] and Seung Min Han*[a]

Received 25th April 2013,
Accepted 27th June 2013

DOI: 10.1039/c3cp51768c

www.rsc.org/pccp

Porous network structures (*e.g.* metal–organic frameworks, MOFs) show considerable potential in dethroning monoethanol amine (MEA) from being the dominant scrubber for CO_2 at the fossil-fuel-burning power generators. In contrast to their promise, structural stability and high-pressure behavior of MOFs are not well documented. We herein report moisture stability, mechanical properties and high-pressure compression on a model MOF structure, MOF-5. Our results show that MOF-5 can endure all tested pressures (0–225 bar) without losing its structural integrity, however, its moist air stability points at a 3.5 hour safety window (at 21.6 °C and 49% humidity) for an efficient CO_2 capture. Isosteric heats of CO_2 adsorption at high pressures show moderate interaction energy between CO_2 molecules and the MOF-5 sorbent, which combined with the large sorption ability of MOF-5 in the studied pressure–temperature ranges show the viability of this sorbent for CO_2 capturing purposes. The combination of the physicochemical methods we used suggests a generalized analytical standard for measuring viability in CO_2 capture operations.

Introduction

Porous solid networks, particularly metal–organic frameworks (MOFs),[1] have long been considered for industrial applications; especially in gas storage and separation since their structures could easily be modified and tuned using a building-block approach resulting in porous materials with low-density and high surface area.[1–6] This approach was shown to prepare a series of MOFs consisting of tetrahedral $[Zn_4O]_6$ units connected *via* organic linkers by reacting carboxylate containing bridging ligands with zinc metal ions.[7,8] A specific compound of this series, named MOF-5 where 1,4-benzene dicarboxylate is used as the bridging ligand, exhibits a BET surface area of up to 3500 $m^2\ g^{-1}$ and a pore volume of 1.31 $cm^3\ g^{-1}$.[9] MOF-5 is arguably one of the most well-studied MOFs[10] and gas uptake studies[10,11] show that it could be a promising candidate in dry CO_2 capture and separation applications. For example, Yaghi *et al.* reported an adsorption value of 22 mmol g^{-1} of CO_2 at 298 K and 40 bar for MOF-5.[11] Further analysis at different temperatures ranging from 220 K to 310 K up to 32 bars has been performed by Simmons *et al.*[12] where 31 mmol g^{-1} of CO_2 was reported as the highest CO_2 capacity (220 K). The adsorption isotherms exhibit negligible hysteresis rendering this compound to be more suitable for capture and separation of CO_2 from flue gases during pre-combustion processes rather than gas sequestration and storage applications. The current dominant technology for removing CO_2 from any power plant is based on a chemical scrubbing process with use of amine-based solvents[13] (*e.g.* monoethanol amine – MEA). The processes that use MEA suffer from high operational costs due to both energy intensive regeneration of the carbonated aqueous solution and the caustic behavior of amine solutions to the steel, leading to alternative methods that use solid sorbents, such as MOFs, to rise to the occasion. Keskin *et al.*[14] assessed CO_2 capture potential of the MOFs with regard to the moist conditions that are commonly found in the exhaust gas mixtures. They concluded that unless MOFs are made immune to the water content of a power plant fume, there would not be a large-scale implementation. An ideal candidate for this task, therefore, is one that could be regenerated easily and is stable under hot and steamy conditions since pre-combustion processes require high pressures (20–50 bar) and warm temperatures (40–70 °C).[15]

Previously, Yaghi and Long reported degradation in the crystallinity of a MOF-5 structure within 10 minutes of exposure

[a] *Graduate School of EEWS, KAIST, 291 Daehak-ro, Yuseong Gu, Daejeon 305-701, Republic of Korea. E-mail: yavuz@kaist.ac.kr, smhan01@kaist.ac.kr; Fax: +82-42-350-2248; Tel: +82-42-350-1718*
[b] *Department of Chemical Engineering, Qatar University, Doha, Qatar. E-mail: mert.atilhan@qu.edu.qa; Fax: +974-4403-4131; Tel: +974-4403-4142*
[c] *Department of Physics, COMSATS Institute of Information Technology, Islamabad 44000, Pakistan*
[d] *Department of Chemistry, University of Burgos, Burgos 09001, Spain*
† Equal contribution.

to air[16] where surface area change was not monitored. Matzger compared common MOFs with respect to their water stability[17] and found that MIL-100 (Cr-BTC) is far more stable than MOF-5, MOF-177, HKUST-1, MOF-505, and UMCM-150, although their study does not report any relationship to a CO_2 capture capacity. They also reported that each of the MOFs they tested, including MOF-5, showed appreciable stability against water for 1 hour. Other reports included a molecular dynamics simulation showing that stability of MOF-5 is lost over >4% water,[18] an MOF-5 analogue called MOCP is deemed unstable in moisture/water,[19] and an excellent review on mechanical properties of hybrid structures.[20] In all these studies, however, the surface area loss analysis over time, high pressure CO_2 capacity, and evaluation of the mechanical properties of the framework to make a judgment on whether MOF-5 could be used for CO_2 scrubbing were not previously conducted. Lessons learnt from this model framework will lead into a generalized method to test other MOFs and perhaps all porous structures.

In this work, we carried out three stability tests on MOF-5: (1) surface area loss when interacting with moist air, (2) mechanical properties analysis using nanoindentation, (3) high pressure CO_2 adsorption. MOF-5 was tested using the MTS XP nanoindenter to evaluate the mechanical properties, and CO_2 adsorption tests were performed *via* a Rubotherm magnetic suspension sorption apparatus (MSB) for adsorption profiles at three different isotherms (318, 328, and 338 K) up to 225 bar. To the best of our knowledge, this work is the first systematic study of monitoring the surface area with respect to the exposure to moist air, and we found that MOF-5 is stable up to 3.5 hours contrary to the common belief, that is enough to carry out several PSA operations and/or transport. Our nanoindentation study was performed within the stability time window before the structural collapse occurs upon exposure to air as determined from the surface area monitoring results. Furthermore, our CO_2 adsorption was recorded up to the highest pressures of CO_2 ever applied on MOF structures, and our results indicate that MOF-5 showed reversible CO_2 uptake without structure collapse at 225 bar.

Materials and methods

Chemicals and materials

Benzene-1,4-dicarboxylic acid (98%), zinc nitrate hexahydrate (98%), *N*,*N*-diethylformamide (DEF) (99%) and chloroform (≥99%) were procured from Aldrich and used as received. Carbon dioxide (≥99.9%) was purchased from Buzwair Gas Company and used as received.

Synthesis, characterization and activation of MOF-5

A solid mixture of $Zn(NO_3)_2{\cdot}6H_2O$ (133.9 mg) and benzene-1,4-dicarboxylic acid (24.9 mg) was dissolved in 5 mL of DEF in a 20 mL glass vial to obtain a highly transparent, light golden yellow solution. The vial was tightly capped and left undisturbed for heating at 85 °C in an oven for 24 h to yield pale yellow square shaped crystals. After cooling the vial to room temperature, the dark golden yellow solution was decanted, and the crystals were washed three times with 20 mL of fresh *N*,*N*-diethylformamide. The crystals were then immersed in 20 mL of chloroform for three days, during which time the activation solvent was decanted and freshly replenished three times. The product was then dried under vacuum at room temperature for 2 hours, and further heated at 120 °C for 6 hours. The diffraction pattern of MOF-5 was recorded using a Rigaku (D/Max-2500) HR-X-ray diffractometer at 40 kV and 300 mA. Measurement was performed for 2θ in the range of 2° to 40° with a step size of 0.01° and a scan speed of 2° min^{-1}. TGA measurement of as-synthesized and activated MOF-5 was carried out on a NETZSCH TG 209 F3 thermogravimetric analyzer at a heating rate of 10 °C min^{-1} under a nitrogen atmosphere. Thin KBr pellets of crystal samples were employed to record IR spectra over the range 4000–550 cm^{-1} at a resolution of 4 cm^{-1} using an FT-IR Spectrometer, Model No. FT-IR 4100 manufactured by Jasco. Nitrogen adsorption–desorption isotherms were measured at 77 K using a Tristar 3020, Micromeritics (USA) porosimetry analyzer. For surface area determination, the Brunauer–Emmett–Teller (BET) method was employed using a nitrogen molecule surface area of 0.162 nm^2. A Tristar 3000 V6.05 A, Micromeritics (USA) porosimetry analyzer was used to determine CO_2 adsorption. The activated samples were degassed for 6 h at 120 °C under vacuum for both sorption measurements. During the moisture stability experiments, temperature and humidity were measured using a Digitales Thermo-Hygrameter, TFA-Germany.

Adsorption measurements

For carbon dioxide adsorption measurements, a high-pressure magnetic suspension sorption apparatus (MSB) made by Rubotherm Präzisionsmesstechnik GmbH was used.[21] The MSB apparatus is rated up to 350 bars at 100 °C. MSB has two different operation positions. First, the measurement cell is filled with CO_2 gas, and MSB records the weight change of the sample that is placed in the sample container as the high-pressure gas is adsorbed by the sample. The second measurement position is used to measure the *in situ* density of the high-pressure gas, which is required to calculate the amount of the adsorbed gas onto the sample in the high-pressure cell. A force transmission error analysis on the high-pressure density measurements was also conducted.

Temperature fluctuations are quite important to achieve constant gas properties during the adsorption process. Therefore double layer thermo-stated baths with active and inactive temperature controlling shields were used to maintain the temperature ±0.6 °C accuracy (Jumo® DMM 5017 Pt100) attached to the high-pressure cell body.

The pressure measurements have ±0.01% full-scale accuracy throughout the measurements (Paroscientific® Digiquartz 745-3 K). The pressure transducer is located near the high-pressure cell and the connection is made *via* a 1/16-inch tube. The dead volume amount is minimized and it is negligibly small.

Nanoindentation

The MOF-5 crystals were adhered to a sample holder using cyanoacrylic adhesive immediately after activation, and nanoindentation tests were performed within the stability window before pore collapse, which occurs at 3.5 hours after exposure.

Nanoindentation tests were carried out using an MTS XP nanoindenter with a Berkovich tip at a nominal constant strain rate ($\dot{P}/P$) of 0.05 s^{-1} in the continuous stiffness measurement (CSM) mode with 2 nm amplitude oscillations to collect contact stiffness (S) as well as load (P), continuously during the depth of indentation (h). Since the MOF-5 crystals form microcracks immediately after activation, the continuous measurements of stiffness were important for determining reliable data sets to probe mechanical properties of the pristine MOF-5 structure, as explained more in detail in the following section.

Results and discussion

If MOFs are going to be used in any CO_2 scrubbing, they will have to go through thorough screening with respect to their (1) structural stability of the pores under moist air, (2) mechanical properties and stability and (3) high pressure compression. Since MOF-5 crystals are known to be sensitive to moisture, it is expected that the crystal degrades and results in macroscopic crack formation after a few hours after activation. Therefore, we first determined the stability window of MOF-5 upon exposure to air using BET and FT-IR analyses.

Stability

As post-combustion CO_2 capture requires water stability, MOFs are expected to withstand moist conditions before being considered for an industrial CO_2 scrubbing operation.[14] In order to assess their potential, we monitored MOF-5's surface area loss as it is the ultimate indicator of structural integrity for gas capture operations since the pore content is critical for the guest gas molecule adsorption.[22] It is anticipated that an acidic gas like CO_2 (especially under humid conditions) may break basic Zn–O bonds at moderate to high pressures. For example, Yaghi *et al.* reported that the crystallinity of MOF-5 degraded within 10 minutes of exposure to moist air as monitored by X-ray diffraction.[16]

The structural collapse due to moist air was fully evaluated in this study using detailed BET and FT-IR analyses. Fig. 1 shows that there is a complete collapse in the pore structure that results in a drop in surface area from 2547.9 $m^2\ g^{-1}$ at 3.5 hours to 37.6 $m^2\ g^{-1}$ after 7 hours of exposure to ambient air at 21.6 °C and 49% humidity (min: 17.2 °C, 39% and max: 24.5 °C, 52%). Further conformation is shown in FT-IR results that indicate growth of –OH and –COOH peaks as the exposure time was increased. As MOF-5 interacted with the moisture in the air, the Zn–O bonds were broken according to the possible mechanisms shown in the following equation:[23,24] (ignoring associated hydrolysis reactions)

$$(Zn_4O)(BDC)_3 + 4H_2O \rightarrow [(Zn_4O)(H_2O)_4(BDC)_2]^{2+} + BDC^{2-}$$

Therefore, the BET and FT-IR results indicate that the maximum air stability window for MOF-5 structure is within 3.5 hours of activation.

Nanoindentation

The mechanical properties of MOFs are of critical importance in applications for CO_2 storage since the sorbents and stored gases usually experience elevated and cyclic pressures, *e.g.* in transport, compression, and decompression.[25] Nanoindentation is one of the widely used techniques for determining the modulus and hardness of materials in small scale volumes,[26] and thus is the suitable technique for probing non-cracked regions within the MOF-5 crystals with external dimensions of the sub millimeter scale. In order to collect reliable data for analysis before structural collapse occurs upon exposure to moist air, we performed our nanoindentation studies within 3 hours of activation, as our stability tests indicated that MOF-5 structure is fully intact within that time frame.

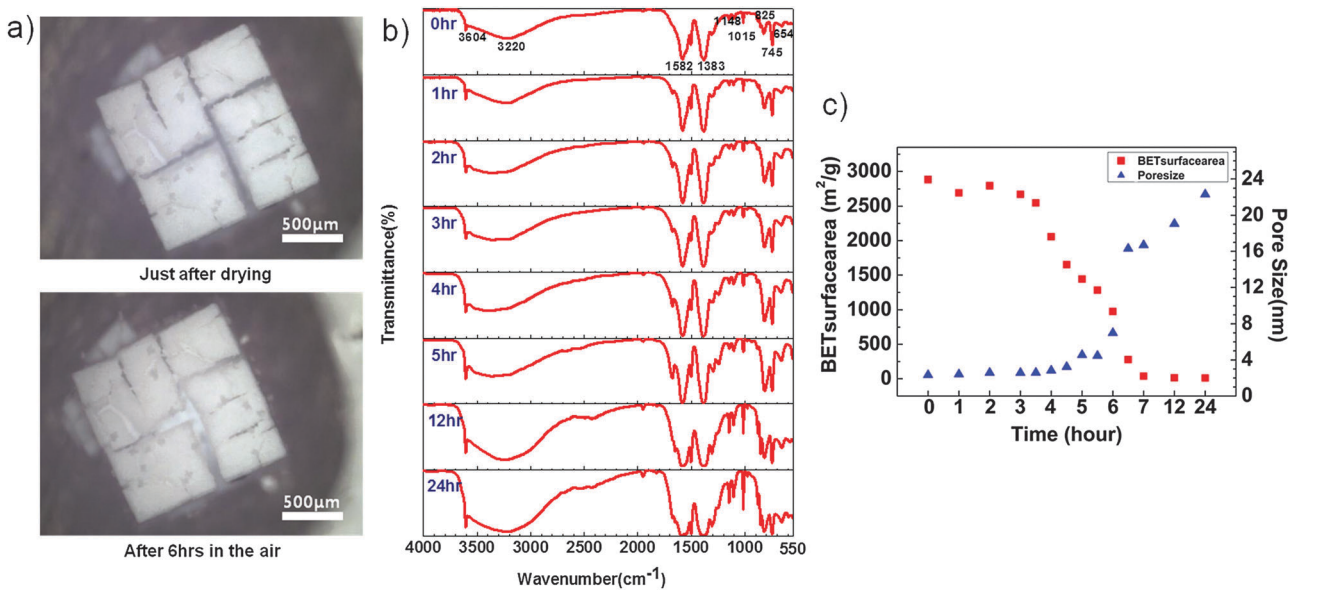

Fig. 1 (a) Optical micrographs showing increased amounts of crack formation after 6 hours of air exposure, (b) time-dependent FT-IR analysis, (c) BET surface area and the average pore size change by time, showing collapse of the pore structure after 3.5 hours of exposure to air.

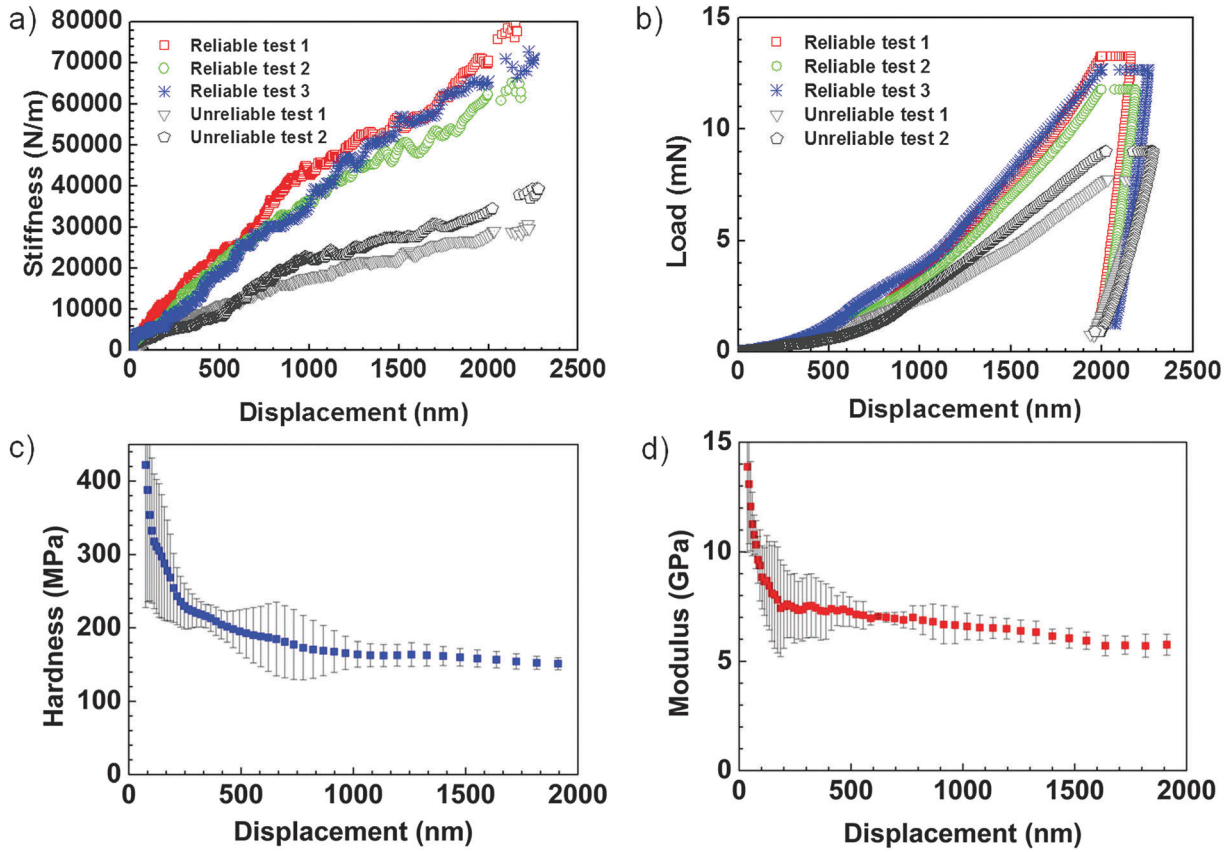

Fig. 2 Nanoindentation result measured within 3.5 hours of exposure to air (a) *S vs. h*, (b) *P vs. h*, Oliver and Pharr (c) hardness and (d) modulus.

The nanoindentation results for the representative contact stiffness (S) *vs.* indentation displacement (h) and load (P) *vs.* displacement (h) plots of MOF-5 crystals within the 3 hour stability time window are shown in Fig. 2a and b. Fig. 2 demonstrates that there is a distribution in the measured P *vs.* h and S *vs.* h response even though the data was collected within the stability window determined from the BET analysis. This distribution in the measured response is likely due to already existing microcracks that were not visible with the optical microscope, which was used to position the indents. Since it is difficult to find pristine regions without any microcracks by using the optical microscope, we used post-testing examination of contact stiffnesses to find reliable data sets for modulus and hardness evaluations. In the absence of any artifacts in the sample due to the microcrack formations, the contact stiffness measurements are expected to be linear with displacement for a Berkovich tip indentation as given by Sneddon's relation,[27]

$$S = 2\beta E_r a \quad (1)$$

where $\beta = 1.034$ for a Berkovich tip, a is the contact radius, and E_r is the reduced modulus as given by

$$E_r = [(1 - \nu_s^2)/E_s - (1 - \nu_i^2)/E_i]^{-1} \quad (2)$$

where ν_s and ν_i are the Poisson's ratios of the sample and the diamond tip, respectively, and E_s and E_i are the Young's modulus of the sample and the diamond tip, respectively. For an elastically homogeneous material with a constant E_r, the stiffness should then be linearly proportional to h since the contact radius a itself is linearly proportional to indentation displacement h. If indentation is performed with the presence of the microcracks or if microcracks were to form during indentation, a reduction in stiffness with displacement will occur and therefore S will start to deviate from the ideal linear behavior with h. Fig. 2a shows a few examples of such tests with reduction in stiffness with displacement. For comparison, repeatable, reliable tests showing linear behavior of S *vs.* h are shown together in Fig. 2a that clearly indicates that unreliable tests result in lower stiffness throughout the depth of indentation. Therefore, we have chosen to work with the repeatable data set that resulted in a linear relationship between S *vs.* h for evaluating the hardness and modulus.

The Oliver and Pharr method of analysis,[26] which is the most widely used method in nanoindentation for homogeneous materials, was used to analyze the repeatable, reliable data to determine the hardness and reduced modulus. The Oliver and Pharr modulus and hardness is determined by

$$H_{OP} = P/A_c(h_c) \quad (3)$$

$$E_r = \frac{\sqrt{\pi}S}{2\beta\sqrt{A_c(h_c)}}, \quad \text{where } E_{OP} = (1 - \nu_s^2)\left[\frac{1}{E_r} - \frac{(1 - \nu_i^2)}{E_i}\right]^{-1} \quad (4)$$

Here, E_i and ν_i are modulus and Poisson's ratio for the diamond tip, and ν_s is the Poisson's ratio of the sample that

was estimated to be 0.3, which is a typical value for polymers. $A_c(h_c)$ is a pre-calibrated area function from fused silica indentation as given by:

$$A_c(h_c) = C_0 \cdot h_c^2 + C_1 \cdot h_c + C_2 \cdot h_c^{\frac{1}{2}} + C_3 \cdot h_c^{\frac{1}{4}} + C_4 \cdot h_c^{\frac{1}{8}}, \quad \text{where } h_c = h - \varepsilon\frac{P}{S} \tag{5}$$

and ε and β are dependent on the geometry of the diamond tip and are given by $\varepsilon = 0.75$ and $\beta = 1.034$ for the Berkovich tip. Results from the Oliver and Pharr hardness and modulus are shown in Fig. 2c and d. Both of the H_{OP} and E_{OP} plots show a wide plateau at large indentation depths, and therefore H_{OP}, E_{OP} of the MOF-5 were taken within the plateau region at an indentation depth of 1 μm where $H_{OP} = 162 \pm 14$ MPa and $E_{OP} = 6.3 \pm 0.45$ GPa. Our results for H_{OP}, E_{OP} of the MOF-5 are higher than those reported by Bahr *et al.*,[28] and we believe that the discrepancy is due to the highly degradable nature of MOF-5 upon exposure to air that causes scatter in the measured results. We believe that our method of analysis by selecting only the data within the stability window as determined using BET analysis and then selecting only a reliable data set with a linear S *vs.* h and constant P/S^2 *vs.* h results in measurement of the true mechanical properties of the MOF-5 porous structure before the pore collapse occurs.

The measured hardness of the MOF-5 crystal can be used to estimate the yield strength by using Tabor's relation,[29,30] where

$$\sigma^{YS} = H/2.7 = 61 \text{ MPa} \tag{6}$$

Here, the Tabor factor of 2.7 was calculated based on the measured hardness and modulus as explained by Feng *et al.*[31,32] The measured strength and modulus of the MOF-5 indicate that MOF-5 is a high strength and modulus material considering that the MOF-5 is a porous structure that mostly consists of polymer chain linkers. One of the common polymer materials of bulk polyvinyl chloride (PVC) can be used for comparison. PVC with density in the range of 0.785–1.52 g cm^{-3} has yield strengths of 35.2–53.4 MPa and moduli of 1.90–3.30 GPa, while the foam grade PVC with density in the range of 0.0404–1.56 g cm^{-3} has dramatically reduced yield strengths of 0.103–0.414 MPa and moduli of 0.0320–1.26 GPa.[33] In comparison to PVC, it is clear that MOF-5 with $\sigma^{YS} = H/2.7 = 61$ MPa and $E_{OP} = 6.3 \pm 0.45$ GPa has significantly higher strength and modulus for a low density porous polymer (0.59 g cm^{-3}),[34] and the strengthening can be attributed to the fact that this is a crystalline polymer, where the ordered structure is able to withstand higher mechanical loadings. The high strength and modulus results indicate that this material is suitable for CO_2 uptake at elevated pressures. However, it should be noted that the observed strength and modulus would only be sustained if the exposure of MOF-5 to moist air were kept under 3.5 hours.

Adsorption measurements

In order to measure CO_2 capture capacities of MOF-5 accurately, we used gravimetric analysis[35] where a magnetic sorption apparatus collects the sorption data based on *in situ* direct buoyancy measurements and gives direct weight change measurements of the adsorbent due to the amount of gas adsorbed on the surface. During the *in situ* sorption measurements, density of the gas that is being adsorbed on the surface is measured by using the magnetic suspension assembly at the same temperature and pressure conditions of the sorption process, as the density of the gas has a direct effect on the calculation of the adsorbed amount. We also check the reliability of the *in situ* density measurements by using the reference equation of state for the gas that is being used (*e.g.* CO_2 in this case) *via* REFPROP 9.1 software, which is the current benchmark for thermo-physical properties of the pure and mixture gases developed by NIST. Moreover, a force transmission error analysis on the high pressure density measurements was also conducted by using the technique published by Cristancho *et al.*[36]

The weight gained by the sample within the high pressure cell is transmitted *via* the contactless method by using magnetic suspension coupling from a closed and pressure-proof metal container to an external microbalance.[37] The measurement cell is equipped with a platinum resistance thermometer Jumo DMM 5017 Pt100 that records temperature of the measuring cell within ±0.6 °C accuracy. Pressure is monitored *via* Paroscientific® Digiquartz 745-3 K with an accuracy of 0.01% in pressure on the full scale. Typical measurements start with placing approximatey 0.25 g of the sample of interest within the sample holder. First the system is kept under vacuum for 24 h at 65 °C. Carbon dioxide is then pressurized *via* a Teldyne Isco 260D fully automated gas booster and charged into the high-pressure cell in order to let carbon dioxide adsorption on the sample begin. For each pressure point it takes about 45 minutes to reach calibration and once temperature and pressure equilibrium is reached, 4 different sets of measurements are taken for a period of 10 minutes at every 30 seconds and the total duration of each temperature and pressure point takes about 50 minutes. At the end of each pressure point, the system goes to the next pressure measurement point automatically. In this work, a pressure of up to 225 bars is used for maximum pressure and at the end of each isotherm, hysteresis check is conducted at each isotherm by collecting desorption data as the system is depressurized.

Adsorption data are analyzed and the amount of adsorbed carbon dioxide on the sample is calculated by using the equation below:

$$W + W_{buoy,sample} + W_{buoy,sink} = m_{ads} + m_{sample} + m_{sink},$$
$$W_{buoy,sample} = (V_{sample} + V_{ads}) \times d_{gas},$$
$$W_{buoy,sink} = V_{sinker} \times d_{gas}, \tag{7}$$

where W is the signal read by the instrument, $W_{buoy,sample}$, $W_{buoy,sink}$ are the buoyancy correction due to the sample and the sinker, and V_{sample}, V_{ads}, V_{sinker} are volumes of the sample, adsorbed gas, and the sinker, respectively. d_{gas} is the density of the gas, and m_{sample}, m_{ads}, m_{sample} are the mass of the sample and adsorption gas, and the sinker, respectively. As mentioned before, MSB is capable of *in situ* density measurements of the gas (d_{gas}), which is collected simultaneously with the sorption data. Both sorption and the density data are used in eqn (7) to

determine the total mass of the adsorbed gas. The mass of the empty sinker ($W_{buoy,sink}$) was measured using helium at several pressures to correct for the buoyancy errors. Volume of the sinker (V_{sinker}) is then calculated from the slope of weight of the sinker *vs.* density plot obtained from this measurement. A blank measurement under vacuum was performed to determine the mass of the sinker (m_{sink}). The buoyancy correction due to the sample ($W_{buoy,sample}$) was performed by calculating the volume of the sample (V_{sample}) from the crystallographic density of the sample.[38] Mass of the sample is determined by performing a measurement under vacuum.

Buoyancy correction of adsorption data

The raw MSB adsorption data contain errors due to lack of understanding of the variations in the volume changes of the sample and the sample holder at high pressures and variable temperatures, which in turn affects the buoyancy of the sample. As the MSB uses the buoyancy basics to determine the amount of gas that is adsorbed, corrections are needed to account for errors that come from buoyancy effects.

The mass of the adsorbed gas m_A is determined from the experimental measurements using the following relationship:

$$m = m_A + m_S + m_{SK} - W_A - W_S - W_{SK} \quad (8)$$

where Δm stands for the experimental readings, m_A, m_S, m_{SK} and W_A, W_S, W_{SK} are the mass and buoyancy correction for adsorbed gas (CO_2), the adsorbent (MOF-5), and the sinker, respectively. Buoyancy corrections are then calculated according to eqn (9)–(11):

$$W_A = V_A d_{gas} \quad (9)$$

$$W_S = V_S d_{gas} \quad (10)$$

$$W_{SK} = V_{SK} d_{gas} \quad (11)$$

where V_i stands for the corresponding volume.

Sample and sinker contributions may be calculated as in previous works. The problem arises in the V_A calculation. Several approaches have been proposed in the literature. Some authors considered the adsorbed phase as having a similar density to the liquid phase of the adsorbate molecules at saturation temperature and ambient pressure.[39,40] Nevertheless, further studies showed that this approach is not valid for high pressures,[35,41] and the use of pore volume in the buoyancy correction of adsorbed gas was proposed, although this is a simplified approach. Dreisbach *et al.*[35] proposed an approach to compute W_A that we have applied to analyse our data with minor modifications.

From eqn (10) and (11), W_S and W_{SK} may be straightforwardly calculated from the experimental $d_{gas}(p,T)$ data if V_S and V_{SK} are assumed to not change in the studied pressure–temperature ranges. Considering eqn (9)–(11) in eqn (8) we obtain:

$$\Delta m = m_S + m_{SK} - V_S d_{gas} - V_{SK}\, d_{gas} + m_A + V_A d_{gas} \quad (12)$$

All the terms except those relating to adsorbed gas with subscript A may be calculated from experimental data, thus:

$$C = m_S + m_{SK} - V_S d_{gas} - V_{SK} d_{gas} \quad (13)$$

$$\Delta m - C = m_A + V_A d_{gas} = m_A + (m_A/d_A) d_{gas} = m_A(1 - d_{gas}/d_A) \quad (14)$$

where d_A stands for the density of adsorbed gas as a function of pressure and temperature, $d_A(p,T)$. As proposed by Dreisbach *et al.*[35] d_A may be calculated using an analytical isotherm model to describe m_A, and thus, through the fit of eqn (14) to experimental data we may obtain the analytical model parameters together with d_A, which will be used in the calculation of W_A.

We have considered a simple Langmuir model to describe m_A:

$$m_A = m_\infty \alpha (b d_{gas})^\alpha / (1 + (b d_{gas})^\alpha) \quad (15)$$

where m_∞, α and b are model parameters. Therefore, substitution of eqn (15) in eqn (14) leads to:

$$\Delta m - C = m_\infty \alpha (b d_{gas})^\alpha / (1 + (b d_{gas})^\alpha)\ (1 - d_{gas}/d_A) \quad (16)$$

Hence, plotting $\Delta m - C$ as a function of d_{gas} and fitting the data to eqn (16) allow us to obtain d_A as an additional fitting parameter together with m_∞, α and b. To obtain d_A as a function of pressure and temperature, we considered each isotherm and fit data to eqn (16) using different, maximum pressures and thus, d_{gas} was obtained as a function of pressure for each isotherm. We show in Fig. 3 an example of the plot of $\Delta m - C$ as a function of d_{gas} together with the fit to eqn (16).

Therefore, we obtain d_{gas} as a function of pressure for each isotherm, results reported in Fig. 4 show that d_{gas} obtained through this procedure are linear functions of pressure. We did the fits up to 100 bar because as reported by Dreisbach *et al.*[35] lower pressures do not show linear trends with pressure, and thus, data for these low pressures were corrected using d_{gas} obtained from the linear extrapolation of d_{gas} obtained at higher pressures.

We report in Table 1 the linear fits of d_A as a function of pressure for the studied isotherms. The $\Delta m - C$ term is called surface excess mass, $m_{A,E}$,[41]

$$m_{A,E} = \Delta m - C \quad (17)$$

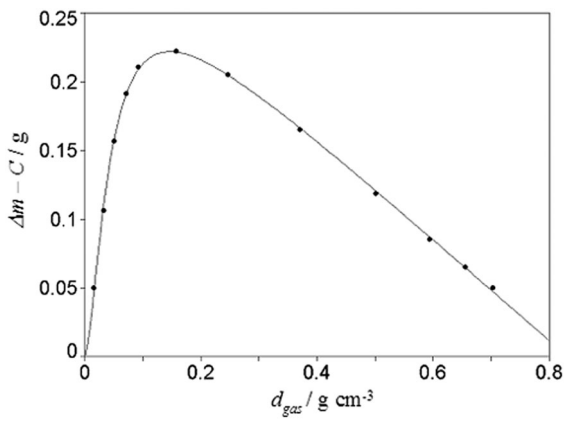

Fig. 3 $\Delta m - C$ as a function of d_{gas} for 343 K using 224.89 bar as the maximum pressure in the fit (fit using data from 9.96 to 224.89 bar). Symbols show experimental data and line fit to eqn (16).

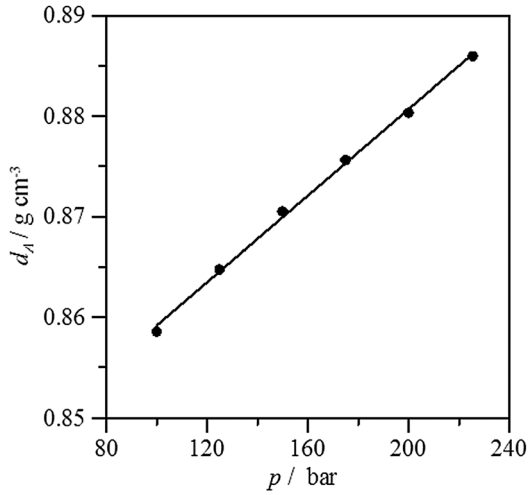

Fig. 4 d_A obtained with the procedure aforementioned as a function of pressure for the 316 K isotherm. Line shows the linear fit of data.

Table 1 Linear fits of density of adsorbed gas, d_A, as a function of pressure for each isotherm, $d_A = ap + b$

	Isotherm		
	316 K	328 K	343 K
a/g cm^{-3} bar^{-1}	0.000215	0.000267	0.000323
b/g cm^{-3}	0.837649	0.799573	0.758151

Therefore, considering parameters reported in Table 1 together with eqn (14) we obtain:

$$m_A = m_{A,E}/(1 - (d_{gas}/d_A)) = m_{A,E}/(1 - (d_{gas}/(ap + b))). \quad (18)$$

Using the corresponding parameters for each isotherm we may obtain the absolute absorbed amount, m_A.

High pressure CO_2 adsorption on MOF-5

We report m_A and $m_{A,E}$ for the three studied isotherms of CO_2 adsorption in MOF-5 in Fig. 5, and our results are compared to the work reported by Millward and Yaghi[11] for comparative purposes in Fig. 5b. In excess surface adsorption (N_{exc}) of MOF-5 up to 225 bar at 318 K, 328 K, and 338 K, V_{ads} was neglected in the work reported by Millward and Yaghi,[11] where it is corrected in the absolute adsorption (N_{abs}) calculations, where N_{abs} is defined as $N_{abs} = N_{exc} + V_{pore} \times d_{gas}$ (V_{pore} is extracted from BET analysis).

Isosteric heat of adsorption

In order to assess the reversibility in CO_2 uptake and the chemical affinity of the sorbent to the guest molecules, the isosteric heat of adsorption is the utmost reference.[14] We obtained the isosteric heat of adsorption data, ΔH_s, from experimental adsorption isotherms using the Clausius–Clapeyron equation. Experimental adsorption data were fitted successfully to a rational type empirical equation,[21] to obtain isosteric data. Calculated heats are reported in Fig. 6 in comparison with available literature information.

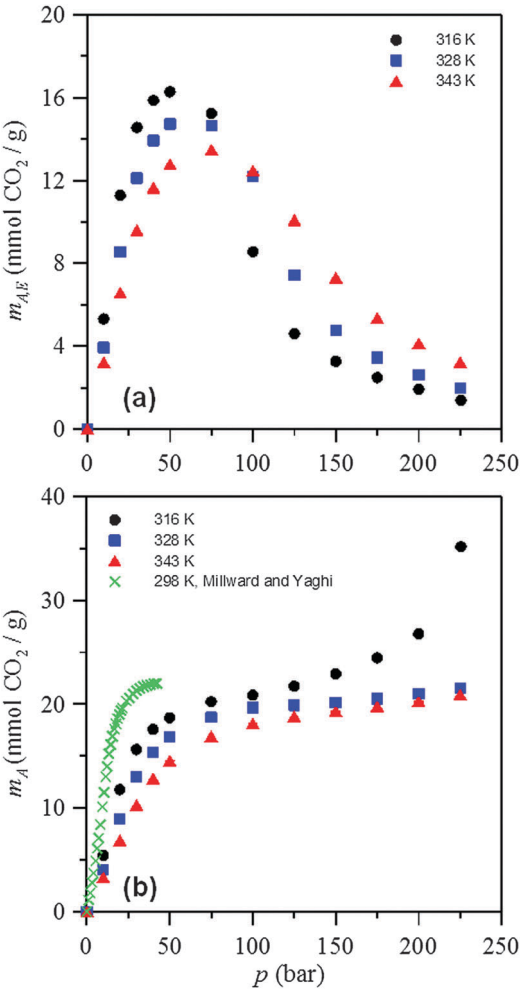

Fig. 5 Excess adsorption amount, $m_{A,E}$, and the absolute adsorption amount, m_A, for CO_2 in MOF-5.

Data obtained in this work are in agreement with literature information for adsorption up to around 15 mmol g^{-1}, but for larger adsorption ΔH_s obtained in this work are larger than those reported by Simmons *et al.*,[12] which are in good agreement with values obtained from Monte Carlo simulations by Babarao *et al.*[42] We should remark that the ΔH_s values reported by Simmons *et al.*[12] were obtained from adsorption isotherms in the 220–310 K range and for pressures up to around 30 bars, whereas the experimental data used for ΔH_s calculations in this work were in the 317–342 K range and using pressures up to 225 bar. The use of these different ranges could be the origin of the differences between our ΔH_s data and those by Simmons *et al.*[12] Moreover, we have used absolute adsorption amounts for ΔH_s calculations, whereas Simmons *et al.*[12] used excess CO_2 sorption isotherms in their calculations. Likewise, we should remark the ΔH_s data reported by Zhao *et al.*[43] for 1.5 mmol g^{-1} (ΔH_s = 34 kJ mol^{-1}), which are twice the value reported by Simmons *et al.*[12]

Isosteric heat of adsorption is a combination of gas–surface (decreasing with increasing pressure) and gas–gas contributions (increasing with increasing pressure).[12] ΔH_s values obtained in

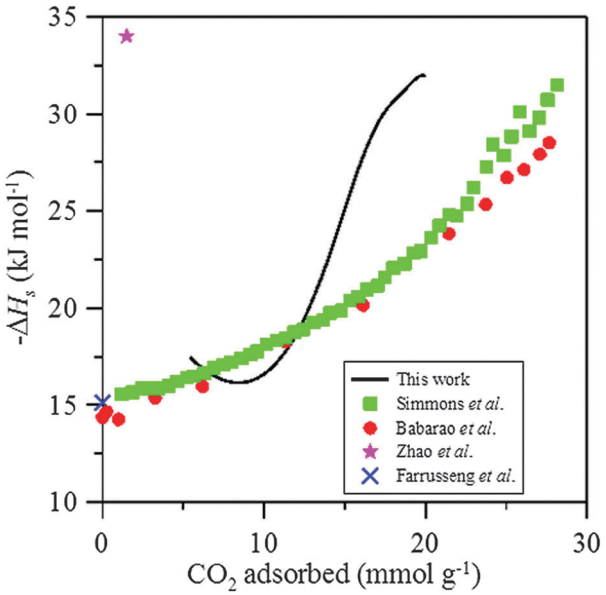

Fig. 6 Isosteric heat of adsorption, ΔH_s, for CO_2 on MOF-5. Literature data obtained from: Simmons *et al.* (Clausius–Clapeyron equation applied in the 220–310 K range),[12] Babarao *et al.* (data obtained from simulations),[42] Zhao *et al.*[43] and Farrusseng *et al.*[44]

this work show a minimum at 8.5 mmol g^{-1} (ΔH_s = 16.2 kJ mol^{-1}) and then increasing ΔH_s values with increasing coverage (ΔH_s = 31.9 kJ mol^{-1} for 20 mmol g^{-1}). The minima may be explained considering that gas–surface contributions prevail over gas–gas ones, with increasing loading gas–surface contribution decreases whereas the gas–gas term does not change remarkably. For larger pressures CO_2–CO_2 interaction begins to prevail over gas–surface ones: the larger the pressure, the closer the adsorbed molecules. Considering the large pressures studied in this work, the gas–gas contributions is expected to be significant, and thus ΔH_s values obtained in this work increase with increased coverage but are larger than those reported by Simmons *et al.* (obtained from lower pressures and lower temperatures).[12] Nevertheless, we should note the very large adsorption ability of MOF-5 coupled with isosteric heat of adsorption. In order to assess the reversibility in CO_2 uptake and the chemical affinity of the sorbent to the guest molecules, the isosteric heat of adsorption is the utmost reference.[14] We obtained the isosteric heat of adsorption data, ΔH_s, from experimental adsorption isotherms using the Clausius–Clapeyron equation. Experimental adsorption data were fitted successfully to a rational type empirical equation,[21] to obtain isosteric data. Calculated heats are reported in Fig. 6 in comparison with available literature information. The moderate heat of adsorption; for example, 20 mmol g^{-1} CO_2 capture may be accomplished at 317 K using only 11 bars of pressure and with 32 kJ mol^{-1} for the heat of interaction. This low interaction energy is less than the half of the interaction energy of CO_2 with the common monoethanolamine solutions used as absorbents.[45] Likewise, even larger CO_2 adsorptions may be obtained using high pressures as the isothermal data reported for the 317 K in Fig. 6.

Conclusions

Metal–organic frameworks (MOFs) are considered among the leading candidates for CO_2 removal from power plant fumes as many nations already started cutting their emissions through renewed regulations.[46] The harsh conditions of exhausts pose risks for highly crystalline substances as mechanical and chemical environments can lead to their complete failure, an undesired outcome.[47] A model MOF structure, MOF-5, was subjected to pore structural stability upon exposure to moist air, measurement of mechanical properties, and confirmation that CO_2 adsorptivity up to 225 bar. Our FT-IR and BET analyses have revealed that one has to stay within the suggested stability window of 3.5 hours of exposure to moist air to avoid structural collapse for reliable gas storage operations. The study of the mechanical properties *via* nanoindentation has shown that MOF-5 has a hardness of 162 ± 14 MPa and a modulus of 6.3 ± 0.45 GPa, which is significantly higher when compared with other porous polymers. Therefore, the MOF-5 material has mechanical properties well suited for CO_2 separation at elevated pressures. In order to confirm the mechanical integrity of the pore structure and the corresponding adsorptivity at elevated pressures, CO_2 capacity of MOF-5 was tested at extreme pressures of 225 bar that indicated fully reversible cycles without any deterioration of the CO_2 capacity. No credible hysteresis also points that a rapid pressure swing adsorption could be envisioned. Lastly, we note that the combination of techniques reported herein has potential to become a generalized method for checking viability of a sorbent for CO_2 scrubbing operations at fossil-fuel power plants.

Acknowledgements

S. M. Han would like to thank the National Research Foundation of Korea under the contract no. 4.0007357, 2011-0014939, 2012K2A1A2033178, and the Center for Inorganic Photovoltaic Materials (no. 2012-0001171) grant funded by the Korean government (MEST). M. Atilhan and C. T. Yavuz would like to thank NPRP grant # 5-499-1-088 from the Qatar National Research Fund (a member of Qatar Foundation) and grants from Korea CCS R&D Center, funded by the Ministry of Education, Science and Technology of Korean government, Basic Science Research Program through the National Research Foundation of Korea (NRF) funded by the Ministry of Science, ICT & Future Planning (2013R1A1A1012998), IWT (NRF-2012-C1AAA001-M1A2A2026588), and KAIST EEWS Initiative.

Notes and references

1 H. Furukawa and O. M. Yaghi, *J. Am. Chem. Soc.*, 2009, **131**, 8875–8883.
2 A. Phan, C. J. Doonan, F. J. Uribe-romo, C. B. Knobler, M. O'Keeffe and O. M. Yaghi, *Acc. Chem. Res.*, 2010, **43**, 58–67.

3 J.-R. Li, Y. Ma, M. C. McCarthy, J. Sculley, J. Yu, H.-K. Jeong, P. B. Balbuena and H.-C. Zhou, *Coord. Chem. Rev.*, 2011, **255**, 1791–1823.
4 Z. Wang and S. M. Cohen, *Chem. Soc. Rev.*, 2009, **38**, 1315–1329.
5 M. Eddaoudi, D. B. Moler, H. Li, B. Chen, T. M. Reineke, M. O'Keeffe and O. M. Yaghi, *Acc. Chem. Res.*, 2001, **34**, 319–330.
6 H. A. Patel, S. H. Je, J. Park, D. P. Chen, Y. Jung, C. T. Yavuz and A. Coskun, *Nat. Commun.*, 2013, **4**, 1357.
7 M. Eddaoudi, J. Kim, N. Rosi, D. Vodak, J. Wachter, M. O'Keeffe and O. M. Yaghi, *Science*, 2002, **295**, 469–472.
8 H. Furukawa, N. Ko, Y. B. Go, N. Aratani, S. B. Choi, E. Choi, A. O. Yazaydin, R. Q. Snurr, M. O'Keeffe, J. Kim and O. M. Yaghi, *Science*, 2010, **329**, 424–428.
9 H. Li, M. Eddaoudi, M. O'Keeffe and O. M. Yaghi, *Nature*, 1999, **402**, 276–279.
10 K. Sumida, D. L. Rogow, J. A. Mason, T. M. McDonald, E. D. Bloch, Z. R. Herm, T.-H. Bae and J. R. Long, *Chem. Rev.*, 2011, **112**, 724–781.
11 A. R. Millward and O. M. Yaghi, *J. Am. Chem. Soc.*, 2005, **127**, 17998–17999.
12 J. M. Simmons, H. Wu, W. Zhou and T. Yildirim, *Energy Environ. Sci.*, 2011, **4**, 2177–2185.
13 G. T. Rochelle, *Science*, 2009, **325**, 1652–1654.
14 S. Keskin, T. M. van Heest and D. S. Sholl, *ChemSusChem*, 2010, **3**, 879–891.
15 D. M. D'Alessandro, B. Smit and J. R. Long, *Angew. Chem., Int. Ed.*, 2010, **49**, 6058–6082.
16 S. S. Kaye, A. Dailly, O. M. Yaghi and J. R. Long, *J. Am. Chem. Soc.*, 2007, **129**, 14176–14177.
17 K. A. Cychosz and A. J. Matzger, *Langmuir*, 2010, **26**, 17198–17202.
18 J. A. Greathouse and M. D. Allendorf, *J. Am. Chem. Soc.*, 2006, **128**, 10678–10679.
19 L. Huang, H. Wang, J. Chen, Z. Wang, J. Sun, D. Zhao and Y. Yan, *Microporous Mesoporous Mater.*, 2003, **58**, 105–114.
20 J. C. Tan and A. K. Cheetham, *Chem. Soc. Rev.*, 2011, **40**, 1059–1080.
21 F. Karadas, C. T. Yavuz, S. Zulfiqar, S. Aparicio, G. D. Stucky and M. Atilhan, *Langmuir*, 2011, **27**, 10642–10647.
22 H. A. Patel, F. Karadas, J. Byun, J. Park, E. Deniz, A. Canlier, Y. Jung, M. Atilhan and C. T. Yavuz, *Adv. Funct. Mater.*, 2013, **23**, 2270–2276.
23 J. A. Greathouse and M. D. Allendorf, *J. Am. Chem. Soc.*, 2006, **128**, 13312.
24 J. J. Low, A. I. Benin, P. Jakubczak, J. F. Abrahamian, S. A. Faheem and R. R. Willis, *J. Am. Chem. Soc.*, 2009, **131**, 15834–15842.
25 H. A. Patel, F. Karadas, A. Canlier, J. Park, E. Deniz, Y. Jung, M. Atilhan and C. T. Yavuz, *J. Mater. Chem.*, 2012, **22**, 8431–8437.
26 W. C. Oliver and G. M. Pharr, *J. Mater. Res.*, 1992, **7**, 1564–1583.
27 I. N. Sneddon, *Int. J. Eng. Sci.*, 1965, **3**, 47–57.
28 D. F. Bahr, J. A. Reid, W. M. Mook, C. A. Bauer, R. Stumpf, A. J. Skulan, N. R. Moody, B. A. Simmons, M. M. Shindel and M. D. Allendorf, *Phys. Rev. B: Condens. Matter Mater. Phys.*, 2007, **76**, 184106.
29 F. J. Baltacalleja and H. G. Kilian, *Colloid Polym. Sci.*, 1988, **266**, 29–34.
30 D. Tabor, *The Hardness of Metals*, Oxford Clarendon Press, New York, 1951.
31 G. Feng, S. X. Qu, Y. G. Huang and W. D. Nix, *J. Mater. Res.*, 2009, **24**, 704–718.
32 G. Feng, S. Qu, Y. Huang and W. D. Nix, *Acta Mater.*, 2007, **55**, 2929–2938.
33 http://www.matweb.com.
34 H. Li, M. Eddaoudi, M. O'Keeffe and O. M. Yaghi, *Nature*, 1999, **402**, 276–279.
35 F. Dreisbach, H. W. Losch and P. Harting, *Adsorption*, 2002, **8**, 95–109.
36 D. E. Cristancho, I. D. Mantilla, S. Ejaz, K. R. Hall, G. A. Iglesias-Silva and M. Atilhan, *Int. J. Thermophys.*, 2010, **31**, 698–709.
37 F. Dreisbach and H. W. Lösch, *J. Therm. Anal. Calorim.*, 2000, **62**, 515–521.
38 W. L. Roberts, T. J. Campbell and G. R. Rapp Jr., *Encyclopedia of Minerals*, Chapman & Hall, New York, 2nd edn, 1990.
39 F. Dreisbach, R. Staudt and J. U. Keller, *Adsorption*, 1999, **5**, 215–227.
40 D. Saha, Z. J. Wei and S. G. Deng, *Int. J. Hydrogen Energy*, 2008, **33**, 7479–7488.
41 H. Furukawa, M. A. Miller and O. M. Yaghi, *J. Mater. Chem.*, 2007, **17**, 3197–3204.
42 R. Babarao, Z. Q. Hu, J. W. Jiang, S. Chempath and S. I. Sandler, *Langmuir*, 2007, **23**, 659–666.
43 Z. X. Zhao, Z. Li and Y. S. Lin, *Ind. Eng. Chem. Res.*, 2009, **48**, 10015–10020.
44 D. Farrusseng, C. Daniel, C. Gaudillere, U. Ravon, Y. Schuurman, C. Mirodatos, D. Dubbeldam, H. Frost and R. Q. Snurr, *Langmuir*, 2009, **25**, 7383–7388.
45 D. Britt, H. Furukawa, B. Wang, T. G. Glover and O. M. Yaghi, *Proc. Natl. Acad. Sci. U. S. A.*, 2009, **106**, 20637–20640.
46 C. T. Yavuz, B. D. Shinall, A. V. Iretskii, M. G. White, T. Golden, M. Atilhan, P. C. Ford and G. D. Stucky, *Chem. Mater.*, 2009, **21**, 3473–3475.
47 S. Zulfiqar, F. Karadas, J. Park, E. Deniz, G. D. Stucky, Y. Jung, M. Atilhan and C. T. Yavuz, *Energy Environ. Sci.*, 2011, **4**, 4528–4531.